

In-situ study of hydride precipitation kinetics and re-orientation in Zircaloy using synchrotron radiation

Authors: K. B. Colas¹, A. T. Motta¹, Y. S. Chu², J.D. Almer², M. R. Daymond³, M. Kerr³, A. D. Banchik⁴, P. Vizcaino⁴ and J. R. Santisteban⁵

1. Department of Mechanical and Nuclear Engineering, Penn State University, University Park, PA USA
2. Advanced Photon Source, Argonne National Laboratory, Argonne, IL, USA
3. Department of Mechanical and Materials Engineering, Queen's University, Kingston, ON, Canada
4. CNEA, Buenos Aires, Argentina
5. CNEA, Bariloche, Argentina

Corresponding author: K. B. Colas, Phone: 1-814-865-9709; Fax: 1-814-865-8499; e-mail address: kuc147@psu.edu

Keywords: Synchrotron radiation, hydride, zirconium alloys, hydride re-orientation

Abstract

The location and orientation of hydrides formed in zirconium alloy nuclear fuel cladding can strongly influence material behavior, mechanical resistance, especially in degradation processes such as delayed hydride cracking. The hydride microstructure is normally studied by post-facto metallography performed at room temperature and without stress. This study uses synchrotron radiation to observe in-situ kinetics of hydride dissolution and precipitation in previously hydrided Zircaloy samples. The hydrogen solubility limit observed in situ was

found to be consistent with literature results [1]. The orientation relationship between hydride platelets and zirconium matrix was confirmed as $\delta(111)//\alpha(002)$. In-situ re-orientation of hydrides was revealed by performing measurements under stress, at temperature. Such experiments showed a characteristic diffraction signature of reoriented hydrides. The results were consistent with a threshold stress for hydride reorientation between 75 and 80 MPa. These results are discussed in light of existing knowledge.

Introduction

Waterside corrosion in light water reactors (LWR) causes hydrogen pickup into the zirconium alloy cladding of the reactor fuel rods. Towards the end of nuclear fuel cladding reactor exposure hydrogen content can reach up to 700 wt. ppm, when the corrosion layer reaches about 100 μm . Since the solubility limit of hydrogen in zirconium is low (below 10 wt. ppm at room temperature) [1], most of this absorbed hydrogen precipitates, forming zirconium hydrides. Most hydrides observed in fuel cladding exposed to reactor environment are delta hydrides ZrH_x with $x\sim 1.6$ [2] but gamma and epsilon hydrides also have been observed [3, 4]. Delta hydrides are platelet shaped [5], and their orientation with respect to the zirconium matrix depends on parameters such as matrix microstructure, temperature and state of stress. Under the influence of stress and temperature gradients, the hydride distribution can become inhomogeneous, such that hydride rims [6], blisters [7] can form which adversely affect cladding ductility. In addition, when a crack is initially present in the cladding under temperature and is stable under the applied stress, hydrogen atoms in solid solution can migrate to and precipitate at the crack tip. The cracking of the hydrides causes advance of the crack which arrests when $K < K_{IC}$ where K is the stress intensity factor and K_{IC} is the fracture toughness in mode I cracking. When the crack reaches unhydrided material, the process starts over. This phenomenon known as delayed hydride cracking (DHC) has been proposed as a

failure mechanism [8-9]. Most analyses of such hydride microstructure changes are performed post-facto, at room temperature and under no stress. It would be of great interest to be able to measure hydride behavior and response to stress in-situ. The aim of this study is to present an in-situ technique for observation of hydride dissolution and precipitation in zirconium alloys. The use of synchrotron radiation from the Advanced Photon Source (APS) at Argonne National Laboratory allows examination of hydride diffraction peaks in-situ with good angular resolution. The beam utilized has high x-ray energy, allowing transmission experiments to be performed, and have load cells and a furnace. These techniques were used to observe hydride re-orientation in the matrix of zirconium alloys as a function of texture and load.

Experimental methods

Two different base alloys were used in this study, Zircaloy-2 and Zircaloy-4 respectively in beam and plate form. The Zircaloy-2 samples of the composition: Zr, 1.43-1.45 wt.% Sn, 0.13-0.14 wt.% Fe, 0.1 wt.% Cr, 0.05 wt.% Ni, 1260-1440 wt. ppm O, 150-160 wt. ppm C, were warm-rolled and recrystallized at Queen's University. The grains are equiaxed and their average diameter is approximately 20 μm . The texture was characterized by obtaining the (0002) and (10 $\bar{1}$ 0) pole figures and calculating the Kearns factors [10]. The (0002) and (10 $\bar{1}$ 0) hcp Zr pole figures are shown on figure 1. The pole figure shows a normal texture, with the basal poles strongly concentrated along the normal direction, with some elements along the transverse direction and little intensity in the rolling direction, as also shown by the Kearns factors which were $f_N=0.887$, $f_T=0.101$ and $f_R=0.012$. The Zircaloy-4 samples prepared by Western Zirconium were cold-rolled in the stress relieved condition. As a result the grains are not equiaxed, but elongated in the rolling direction.

Two types of sample geometry were used in two different orientations. The two different sample geometries are shown in Figure 2(a). The first rectangular plain sheet sample was used for the bulk diffraction experiments, cut in two different orientations. The second, dog-bone type tension sample was used for the in-situ experiments. Since zirconium is crystallographically anisotropic a typical texture (see Figure 1) is induced by rolling, therefore all three directions, rolling (RD), normal (ND) and transverse (TD) are defined. The left hand side of Figure 2(b) illustrates the orientation of the basal planes, found within $\pm 30^\circ$ of the ND direction in the ND-TD plane.

These samples were hydrogen charged by high temperature gas diffusion, for which several steps were needed. First, the native oxide layer existing on the surface of the samples was removed by dipping the samples for 1 min in an acid solution of 1 part HF, 10 parts nitric acid and 10 parts H₂O. Second, using an electron-beam evaporator a thin layer of nickel was deposited onto the sample surface to prevent oxidation [7]. The samples were then charged in a vacuum furnace using a mixture of 12% hydrogen and 82% argon, introduced at 450°C. Several temperature cycles were necessary to obtain the desired level of hydrogen. The total time at 450°C was 3 hours so no significant re-crystallization has occurred. Table 1 summarizes the samples used, and the heat treatment and loading procedure they received for this experiment.

Metallography

Metallography was performed to characterize hydride orientation and to estimate the original hydrogen content using image analysis. The samples were mounted in epoxy casts polished using 140, 400, 800 and 1200 grit silicon carbide paper, and then etched using the same solution used for oxide layer removal. This solution preferentially etched the zirconium hydrides, which allowed their observation using optical microscopy.

Synchrotron X-Ray diffraction

Two different beamlines at the Advanced Photon Source at Argonne National Laboratory were used in this study. The first beamline, 2BM, contains a four circle diffractometer used for general diffraction of previously prepared samples. The samples had received different heat treatments under load but were observed post-facto at room temperature. Figure 3(a) shows the beamline setup. The white X-ray beam is made into a monochromatic beam using filters and monochromators. For our experiment the beam energy was 15 keV. The beam size (1mm x 10mm) is defined by a series of slits. The detector used was a NaI point detector. Figure 3(b) shows the experimental set-up for the in-situ experiments performed at beamline 11D. The samples were observed using transmission X-ray diffraction and a high-speed plate detector was used to collect the data. This geometry allows for the full diffraction rings to be recorded. Thus any in plane texture can be studied. Because obtained in transmission this gives us bulk data averaged over the sample thickness. The obtained diffraction rings are integrated over the whole angular range to obtain diffraction patterns. The beam energy was 80keV and the beam size was 0.3mm x 0.3mm. The samples were placed in a tensile device which could be operated under displacement or force control. The MTS frame used for applying stress to the samples allowed computer monitoring of the applied force (in N), the displacement (in mm), or the displacement rate (in mm/s). The testing temperature was controlled using a furnace and the sample temperature was monitored with an error of $\pm 1^\circ\text{C}$ using K-type thermocouples spot welded onto the sample surface.

Results

The results are presented in two main parts: the metallography and the synchrotron X-ray diffraction experiments. The XRD experiments are of two sorts. The first set of results, performed in reflection geometry consists of post-facto observations of hydrided samples to determine their hydrogen content and the orientation relation of the zirconium hydride platelets to the α -zirconium matrix. The second set of results obtained using transmission XRD consists of in-situ observation of hydride dissolution.

Metallography

Figure 4 shows optical metallographs for the two sample orientations presented in Figure 2(b) and which were used for the post-facto bulk diffraction experiment. The hydrides appear as dark lines on a light matrix. Both samples show hydride platelets lying on the TD-RD plane, but the sample surface normal is ND in Figure 4(a) and TD in Figure 4(b).

In the second set of experiments described in the previous section, the samples were heat treated and stressed in-situ during the diffraction experiment at the synchrotron.

Metallography was performed both before and after the heat treatment and application of stress during XRD experiment allowing us to compare the effect of the experiment on the hydride microstructure.

Figure 5(a) shows a Zircaloy-2 sample containing 600 wt. ppm of hydrogen and has the equivalent texture to that shown in Figure 4(a) and thus the hydrides present the same initial orientation. This sample was inserted in the transmission set-up described in Figure 3(a), heated up to 550°C and then cooled down with an applied tensile load of 75MPa (the tensile load is defined as the force in Newton divided by the cross-sectional area of the sample).

When the temperature is increased, a larger fraction of the hydrogen goes into solution. At

550°C all hydrides are dissolved for samples with 600 wt. ppm of hydrogen. This newly dissolved fraction re-precipitates upon cooling, and if a stress is applied during cooling the orientation of the re-precipitated hydrides may change [11]. No major difference appears between the hydride microstructure before, (Figure 5(a)) and after the experiment (Figure 5(b)). The zirconium hydrides appear to have re-precipitated in a similar orientation to that found before the experiment. In contrast when the same experiment was performed at 85MPa, the final hydride microstructure (Figure 5(d)) is significantly different from the initial one (Figure 5(c)). In the initial stage the hydrides are all oriented parallel to the sample surface, while after heating and cooling under load, a significant fraction of hydrides precipitate with their platelet normal aligned to the load axis.

The dog-bone shape of the specimen enhances the effect of stress by creating stress concentration in the gage section. Figure 6 shows optical metallographs of a Zircaloy-4 dog-bone sample with 600 wt. ppm. This sample was heated to 550°C, then cooled down under a tensile stress of 100 MPa. The sample was cut in its length and different pictures were taken at different locations along the dog-bone shaped sample. Figures 6(a) and 6(d) were taken at the thick end of the sample whereas Figure 6(b) and Figure 6(c) were taken in the gage section which has a much smaller cross-sectional area and thus highest stress. Because of this in the metallographs taken in the gage section, many hydrides have reoriented with the normal to the platelet now parallel to the tensile axis, while in the thick ends of the dog-bone shaped sample hydride orientation has remained the same.

Synchrotron X-Ray diffraction

This section presents the results from the XRD experiments performed at the APS. Figure 7 shows the relative intensity versus two-theta angle acquired in reflection XRD at 15keV for samples with three different hydrogen contents. The diffraction peaks identified are the α -

zirconium matrix peak (100) and the δ -hydride (111) peak. For the sample with the highest hydrogen content the γ -hydride (111) peak can also be observed. The intensity of the α -zirconium (100) peak is relatively similar for the three samples, the small variations observed are due to grain sampling differences. However the δ -hydride (111) peak intensity increases significantly with hydrogen content. This relation can be used to estimate the local hydrogen content of those samples. Figure 8 shows a diffraction pattern acquired for two Zircaloy-2 samples that were cut in two different orientations (ND and TD) as shown in Figure 2(b). The α -zirconium (002) peak is much more intense in the ND than in the TD sample, which is understandable from the orientation of the basal planes of the zirconium matrix relative to the sample surface, shown on the side. For the TD sample the α -zirconium (101) and (100) peaks are more intense than in the ND samples. Both the δ -hydride (111) peak and the δ -hydride (200) peak are observed in Figure 8. The δ -hydride (111) peak is more intense in the diffraction pattern from the ND sample than in the one from the TD sample. On the contrary, the δ -hydride (200) peak is more intense in the diffraction pattern from the TD sample than from the ND sample. This shows that the re-orientation of the hydrides causes the relative intensities of the hydride peaks to shift.

Figure 9 shows diffraction patterns obtained from a Zircaloy-2 sample with 100 wt. ppm of hydrogen in the initial state and acquired in transmission geometry using an energy of 80keV in the initial state. An example of the data obtained using transmission XRD is presented in Figure 9. Such data can be integrated along the rings to give the diffraction intensity as a function of two-theta, as shown in Figure 10. The full diffraction patterns shown in Figure 10 are obtained by integrating along the 360° around the diffraction rings in Figure 9. The samples observed in-situ were heated to a temperature above the solvus, and so the hydrides completely dissolved. Some samples also had a tensile load during cool-down. In Figure 10 the XRD patterns of a Zircaloy-2 sample with 100 wt. ppm of hydrogen are presented for

different temperatures during heating. Figure 11 presents a close-up of Figure 10 in the two-theta region comprised between 3.00° and 3.60° . It is clear that the intensity of the δ -hydride (111) peak decreases with increasing temperature, and also that the α -zirconium (002) peak location shifts towards lower angular values with increasing temperature. The disappearance of the δ -hydride peak is caused by the dissolution of the hydride precipitates. The $\delta(111)$ peak intensity is plotted along with the temperature in Figure 12. The diffraction signal disappears at 330°C , in good agreement with the solvus for 100 wt. ppm of 333°C . The change in peak location is likely related to lattice expansion. The calculated strain between room temperature and 300°C is 1.73×10^{-3} which corresponds well with the strain calculated using lattice expansion of $5 \times 10^{-5}/^\circ\text{C}$ giving 1.35×10^{-3} for a 270°C temperature change.

Figures 13 and 14 present the results for two Zircaloy-4 samples that were heated up to 550°C then cooled down to room temperature under tensile loading. Figure 13 shows a blow-up of the 2θ region near the $\delta(111)$ peak for two samples, before and after heating then cooling down under load, one sample at 85MPa and the other at 100MPa. The $\delta(111)$ peak intensity decreases in both cases, but a larger decrease is observed in the sample with a higher tensile load applied. In figure 14, the same feature can be observed for the $\delta(220)$ peak intensity: it decreases from initial to the final state for the 85MPa sample and it decreases even more for a higher tensile load applied.

Analysis

Estimation of local hydrogen content

The hydrogen contents were estimated using three different techniques. The first technique, the Direct Comparison Method, consists of taking the ratio of the integrated peak intensities

of the $\delta(111)$ peak over the $\alpha(002)$ peak [12]. This ratio can be related to the volume fraction of hydrogen V_δ/V_α by the following equation [13]:

$$\frac{I_{\delta(111)}}{I_{\alpha(002)}} = \frac{R'_{\delta(111)}V_\delta}{R'_{\alpha(002)}V_\alpha} \quad (1)$$

$$R'_{X(hkl)} = \left(\frac{1}{v_X^2} \right) \left[|F_{X(hkl)}|^2 P_{X(hkl)} \left(\frac{1}{\sin^2 \theta_{X(hkl)} \cos \theta_{X(hkl)}} \right) \right] (e^{-2M})_{X(hkl)}$$

where v_X is the volume of the unit cell (m^3), $|F_{X(hkl)}|^2$ is the structure factor for peak hkl , $P_{X(hkl)}$ is the multiplicity factor, $\theta_{X(hkl)}$ is the Bragg angle for the peak considered and $(e^{-2M})_{X(hkl)}$ is the temperature factor, all for each phase X. It should be noted that no hydrides other than δ hydrides were present in the samples used for these calculations, therefore it was not necessary to take into account γ or ϵ hydrides to calculate the total hydrogen content. The second method used was image analysis of the metallography pictures. Using an image analysis software, the optical metallographs were transformed to black and white pictures (black pixels being the hydrides and white background being the zirconium matrix). Then, once the area fraction of hydrides was determined, the hydrogen contents can be estimated after calibration using a sample of known hydrogen content by considering that the volume fraction observed is proportional to the volume fraction (we should note that the area fraction changes with the etching procedure and so a calibration is needed). The third method was the measure of hydrogen content using hot vacuum extraction. The three methods were applied to two Zircaloy-2 samples and the results are shown in Table 2. Considering the uncertainties and possible sources of error, the three methods are in good agreement and can be used to obtain a first-order estimate of the local hydrogen content in the sample.

Kinetics of hydride precipitation

The diffraction patterns presented in Figure 10 and 11 have been manually fit using PeakFit®. A Pearson Voigt VII peak shape was assumed, which allow fitting of the full width half maximum and peak tails independently. A linear background model was used. The fitting obtained were quite good, as shown by the R^2 values obtained, which were consistently above 0.92. The results of the fitting are the peak locations and the integrated intensities of the peaks. The first part of this analysis consists of studying the kinetics of hydride dissolution and precipitation with no stress applied. A Zircaloy-2 sample with initially 100 ppm of hydrogen was heated up to 450°C, held at this temperature for 15 min, then cooled down to room temperature (Figure 11). For the sample presented here the heating and cooling rates are 0.03°C/s. During the heating/cooling stage diffraction patterns were acquired every 10 sec. Three of these patterns are represented in Figure 10 and 11. During dissolution, the in-situ solubility limit is approximately 330°C for 100 wt. ppm of hydrogen. This is in good agreement with the theoretical solubility limit of 348°C for a 100 wt. ppm sample. During cool-down however, hydrogen precipitates at 150°C which is significantly after the theoretical solubility limit of this sample which is 300°C for a 100 wt. ppm sample during precipitation [1].

Influence of stress and microstructure on hydride orientation

In this section, the orientation of the hydrides and its effect on the diffraction pattern is discussed. As shown in Figure 4, for both sample orientations the hydride platelets are parallel to the basal planes in the as-hydrided state. Since a hydride platelet has the $\delta(111)$ pole parallel to its habit plane [14], the macroscopic relationship between the hydride platelets and the zirconium matrix is approximately:

$$\delta(111)//\alpha(0002)$$

in agreement with previous results [14, 15]. Therefore, the texture of the zirconium matrix determines the initial hydride orientation.

The stress applied during cooling has a significant impact on hydride orientation [11]. In the transmission in-situ experiment, several samples containing 600 wt. ppm of hydrogen were heated up to 550°C in order to dissolve all the precipitates, then a tensile load was applied during cool down. As seen on the metallographs (Figures 5 and 6), when a sufficient tensile load is applied to a sample during cooling, the orientation of the hydride precipitates is influenced by the tensile stress direction and not only by the texture of the matrix. The tensile load causes a fraction of the hydride platelets to reorient with their normal parallel to the tensile direction, i.e.:

$$\delta(111)//\text{tensile direction}$$

Figure 6 shows a threshold stress is needed: in the gage section where the tensile stress is highest, the influence of stress on hydride orientation is significant, whereas in the end sections of the dog-bone shaped sample where the stress intensity is lowest, hydride orientation is only influenced by the texture of the matrix. Since re-orientation occurred for samples cooled under 85MPa and not for samples under 75MPa, it is likely the threshold stress is in between these values.

Finally, the diffraction patterns (Figures 13 and 14) show that the higher the tensile load, the greater the degree of hydride re-orientation observed. After re-orientation, the $\delta(111)$ hydride peak intensity decreases, as well as the $\delta(220)$ peak (to a lesser degree). These observations, consistently observed during our experiments allow us to ‘fingerprint’ the hydride re-orientation using X-ray diffraction. We note that it is likely that the habit planes of the hydrides have not changed, and that the changes observed are related to hydride morphology changes, as described by [14].

Conclusions

Detailed X-ray diffraction measurements were performed on various hydrided zirconium alloy samples using synchrotron radiation. The objective of the study was to determine what occurs to a hydride distribution when heated and cooled under load. Both in-situ and ex-situ experiments were performed for samples of different orientations under different levels of load, and the results compared to metallography.

- The determination of hydrogen content by three different methods was in good agreement. The solvus corresponded well the reported solubilities upon heating, and less well upon cooling.
- The initial hydride microstructure and orientation is determined by the zirconium matrix texture and consists of hydride platelets approximately aligned such that $\delta(111)//\alpha(0002)$.
- After high temperature annealing, the hydrides re-orient such that $\delta(111)//\text{load axis}$. This is accompanied by decrease in the intensity of the $\delta(111)$ and $\delta(220)$ peaks. This shift increases with increasing load.
- These results show that it is possible to study hydride dissolution and precipitation and re-orientation using in-situ X-ray diffraction. More detailed studies will follow in the near future.

Acknowledgements

This research was funded by a Materials World Network grant from the National Science Foundation under grant #XXXX, with corresponding funding from NSERC and CONY CET for the Canadian and Argentinean partners. We are grateful for their support. Us of the APS was funded under XXXX.

References

- [1] McMinn, A., Darby, E. C. and Schofield, J. S., Zirconium in the Nuclear Industry: 12th International Symposium, 2000, ASTM STP 1354: pp. 173-195.
- [2] International Center for Diffraction Data, The Powder Diffraction File, 2006.
- [3] Bradbrook, J. S., Lorimer, G. W., and Ridley, N., Journal of Nuclear Materials, 1972, vol. 42, pp. 142-160.
- [4] Beck, R. L., Transactions of the ASM, 1962, vol. 55, pp. 542-555.
- [5] Perovic, V, Weatherly G. C, Simpson, C. J, Acta Metallurgica, 1983, vol. 31, pp. 1381-1391.
- [6] Swam, L. F. Van Strasser, A. A., Cook, J. D., and Burger, J. M., 1997 LWR Fuel Performance Meeting, 1997, Portland, PR, pp. 421-431.
- [7] O. N. Pierron, D. A. Koss, A. T. Motta, K. S. Chan, Journal of Nuclear Materials, 2003, vol. 322, pp. 21-35.
- [8] Petterson, K., Kese, K., and Efsing, P., Proceedings of the 9th International Conference on Environmental Degradation of Materials in Nuclear Power Systems-Water Reactors; The Minerals, Metals and Materials Society, Warrendale, PA, 1999, pp. 1169-1175.

- [9] Grigoriev, V. and Josefsson, B., Journal of Nuclear Materials, 1998, vol. 257, pp. 99.
- [10] Kearns J. J, Woods, C. R., Journal of Nuclear Materials, 1966, vol. 20, p.241.
- [11] Kammenzind, B.F., Berquist, B.M. , Bajaj, R. , Kreyns, P.H. and Franklin D.G, Zirconium in the Nuclear Industry: 12th International Symposium, 2000, ASTM STP 1354: pp. 196-233.
- [12] Daum, R. S, Chu, Y. S. and Motta, A. T., Journal of Nuclear Materials Submitted, 2008.
- [13] Cullity, B. D., Elements of X-Ray Diffraction, Second Edition, Addison-Wesley Publishing Company, Inc, 1978.
- [14] Chung, H. M, Daum, R. S, Hiller J. M. and Billone M. C., Zirconium in the Nuclear Industry: 13th International Symposium, 2002, ASTM STP 1423: pp. 561-582.
- [15] Westlake, D. G., Journal of Nuclear Materials, 1968, vol. 28, pp. 208-216.

Figure captions

Figure 1 Texture of as-received Zircaloy-2. Note that in both plots intensity increases with darkness

Figure 2 (a) Samples microstructural orientations ; (b) Sample geometry

Figure 3 (a) Experimental set-up of beamline 2-BM at the Advanced photon source; (b) Experimental set-up of beamline 1-ID at the Advanced Photon Source

Figure 4 (a) Metallography of Zircaloy-2 sample with 500 wt.ppm hydrogen content and the normal direction coming out of the sample surface; (b) Metallography of Zircaloy-2 sample with 500 wt.ppm hydrogen content and the transverse direction coming out of the sample surface

Figure 5 (a) Metallography of Zircaloy-2 sample with 600ppm of hydrogen; (b) Same sample after being heated up to 500°C then cooled down with a tensile stress of 75 MPa applied; (c) Metallography of Zircaloy-4 sample with 600ppm of hydrogen; (d) Same sample after being heated up to 500°C then cooled down with a tensile stress of 85 MPa applied.

Figure 6 Zircaloy-4 sample 600 wt ppm heated at 550°C then cooled down with 100 MPa applied (a) 2mm from left edge of sample (LE) ; (b) 6mm from LE (gage section); (c) 8 mm from LE (gage section); (d) 12 mm for LE

Figure 7 X-ray diffraction patterns of three Zircaloy-2 samples with hydrogen contents of 0 wt.ppm, 150 wt.ppm and 500 wt.ppm

Figure 8 X-ray diffraction patterns of two Zircaloy-2 samples with different microstructural orientation

Figure 9 X-ray diffraction data obtained in transmission from a Zircaloy 2 sample with 100 ppm of hydrogen

Figure 10 Integrated X-ray diffraction patterns obtained in transmission for a Zircaloy-2 sample with hydrogen content of 100 wt.ppm taken at different temperatures during heating

Figure 11 Close-up of Figure 9 integrated diffraction patterns of a Zircaloy-2 sample with hydrogen content of 100 wt.ppm taken at different temperatures during heating

Figure 12 Evolution of delta (111) hydride intensity with time for a Zircaloy-2 sample with 100 ppm in hydrogen content

Figure 13 Integrated X-ray diffraction patterns obtained in transmission for two Zircaloy-4 samples heated then cooled down under 85 MPa and 100 MPa tensile load: close-up on $\delta(111)$ peak

Figure 14 Integrated X-ray diffraction patterns obtained in transmission for two Zircaloy-4 samples heated then cooled down under 85 MPa and 100 MPa load: close-up on $\delta(220)$ peak

Tables

Table 1 Description of samples used for these experiments (the 4 first samples were observed post facto, the last four were used for in-situ loading and temperature experiments)

Sample reference	Sample material	Sample orientation (direction coming out of surface)	Geometry	Hydrogen content (wt ppm)	Observed in-situ or post-facto?	Applied tensile stress (MPa)	Heat cycle up to (°C)
Sample 1	Zircaloy-2	Normal direction	Bulk	0	post-facto	0	450
Sample 2	Zircaloy-2	Normal direction	Bulk	150	post-facto	0	450
Sample 3	Zircaloy-2	Normal direction	Bulk	500	post-facto	0	450
Sample 4	Zircaloy-2	Transverse direction	Bulk	500	post-facto	0	450
Sample 5	Zircaloy-2	Normal direction	Bulk	100	in-situ	0	450
Sample 6	Zircaloy-2	Normal direction	Tensile	600	in-situ	75	500
Sample 7	Zircaloy-4	Normal direction	Tensile	600	in-situ	85	500
Sample 8	Zircaloy-4	Normal direction	Tensile	600	in-situ	100	500

Table 2 Comparison of direct comparison, image analysis and hot vacuum extraction for estimation of local hydrogen content of zirconium alloys

	Calculated hydrogen contents (wt. ppm)		Measured hydrogen contents (wt. ppm)
	Direct Comparison Method	Image analysis	Hot vacuum Extraction
Zircaloy 2 Sample A	527	588	613
Zircaloy 2 Sample B	153	233	172

Figures

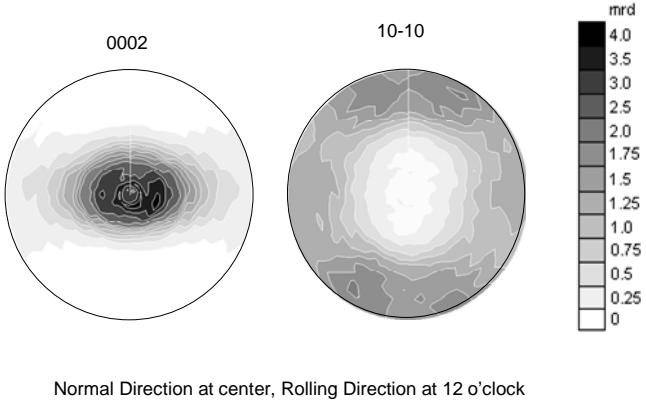


Figure 1: Basal (0002) and prismatic (10-10) pole figures for Zircaloy-2 plate. The intensity scale is shown on the right.

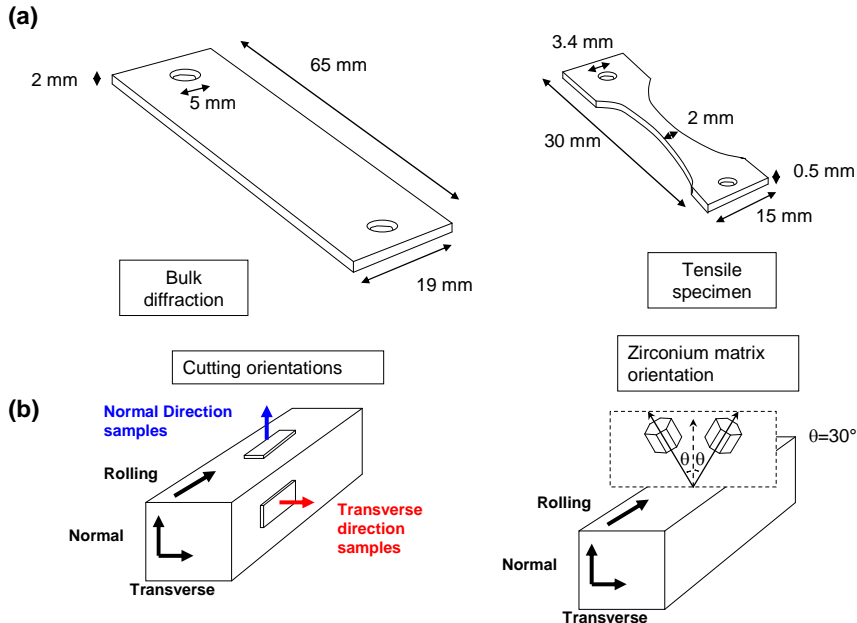


Figure 2 (a) : Sample geometries (bulk diffraction) on left and dog-bone specimen on the right.
 (b) : Sample orientation and matrix texture

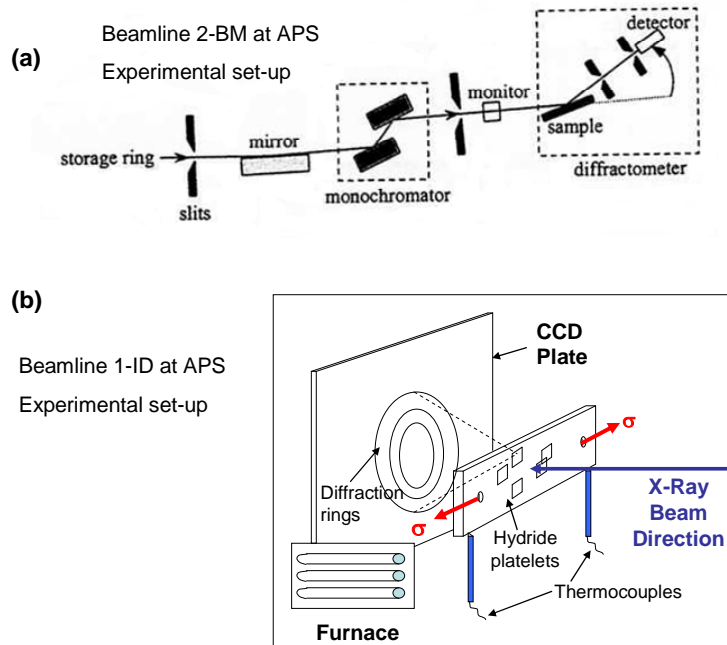


Figure 3 (a) : Experimental set-up of beamline 2-BM at the Advanced photon source. (b): Experimental set-up of beamline 1-ID at the Advanced Photon Source

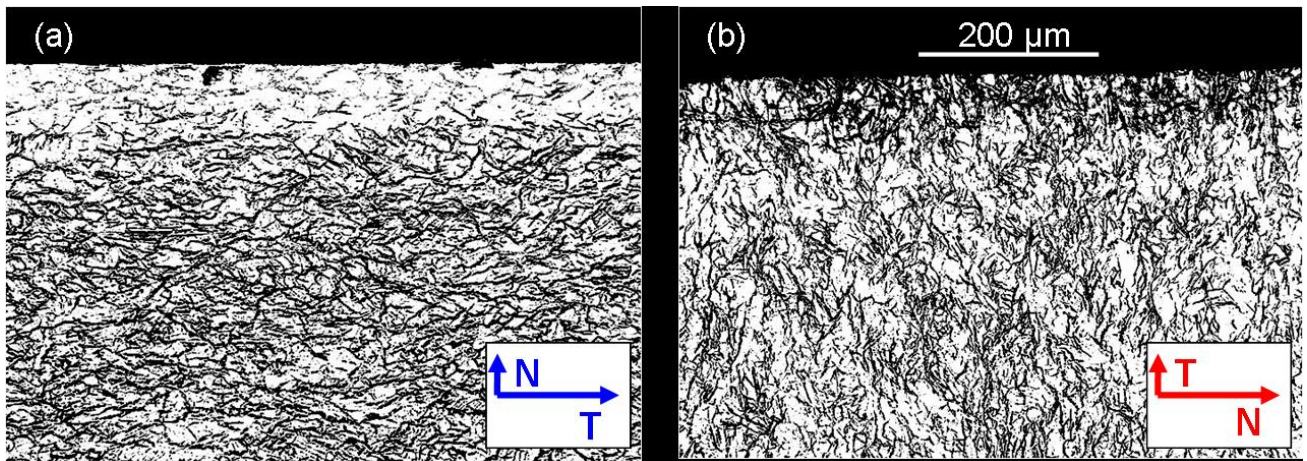


Figure 4 (a) : Metallography of Zircaloy-2 sample with 500 wt. ppm hydrogen content and the normal direction coming out of the sample surface. (b) : Metallography of Zircaloy-2 sample with 500 wt. ppm hydrogen content and the transverse direction coming out of the sample surface.

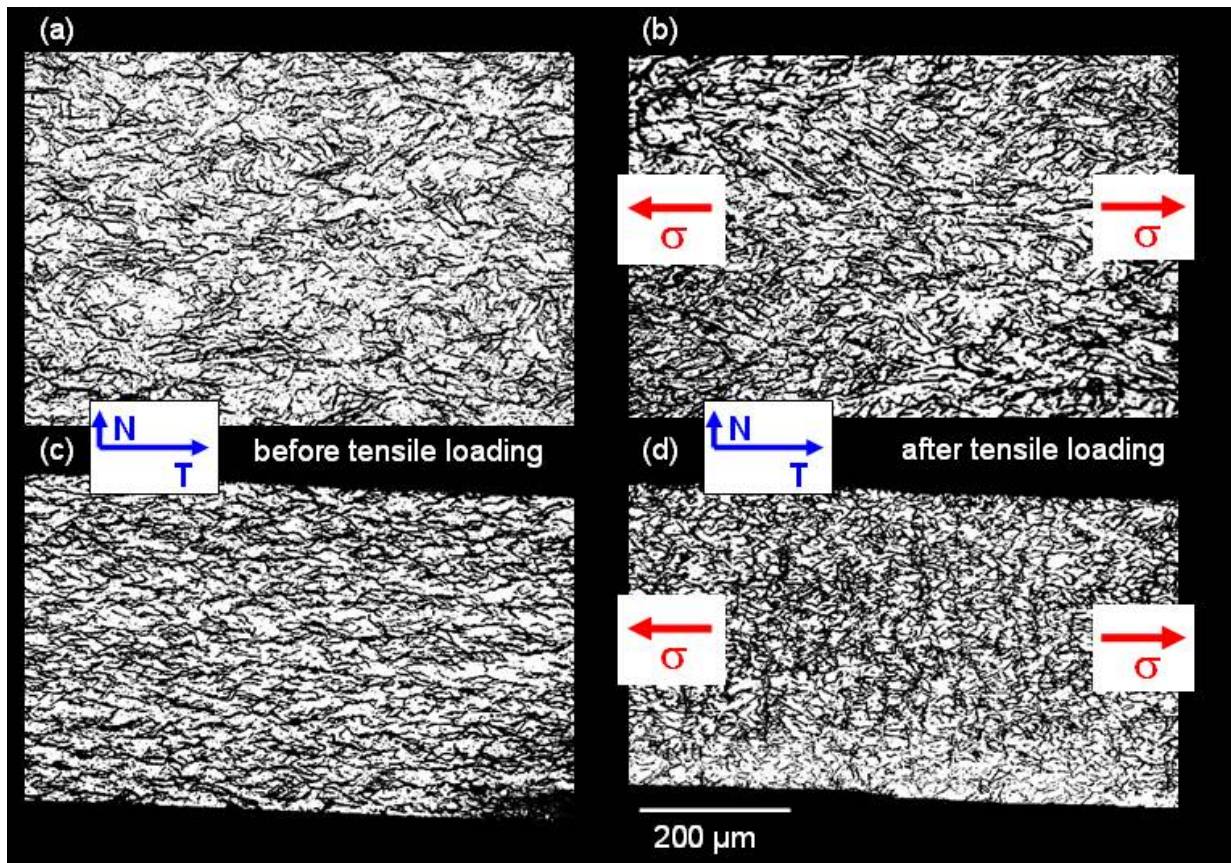


Figure 5 (a) : Metallography of Zircaloy-2 sample with 600ppm of hydrogen. (b) : Same sample after being heated up to 500°C then cooled down with a tensile stress of 75 MPa applied. (c) : Metallography of Zircaloy-4 sample with 600ppm of hydrogen. (d) : Same sample after being heated up to 500°C then cooled down with a tensile stress of 85 MPa applied.

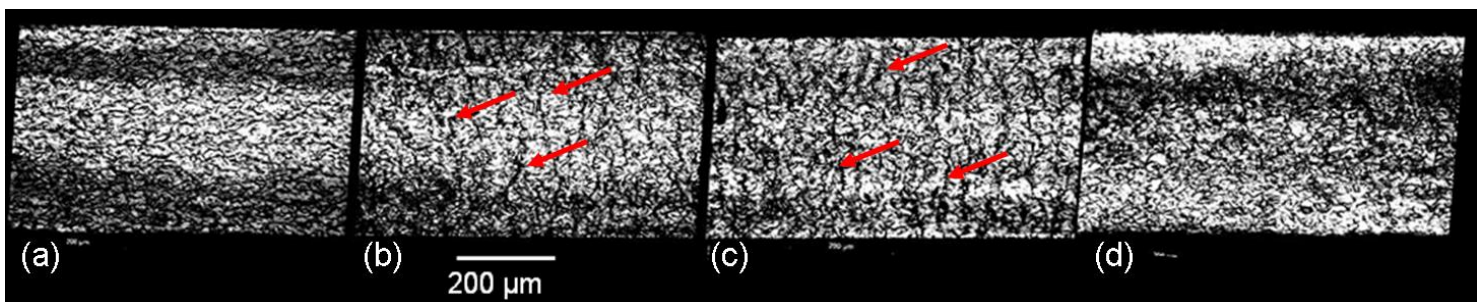


Figure 6: Zircaloy-4 sample 600 wt ppm heated at 550°C then cooled down with 100 MPa applied (a): 2mm from left edge of sample (LE). (b) : 6mm from LE (gauge section) (c) : 8 mm from LE (gauge section). (d) : 12 mm for LE (the arrows indicate re-oriented hydrides)

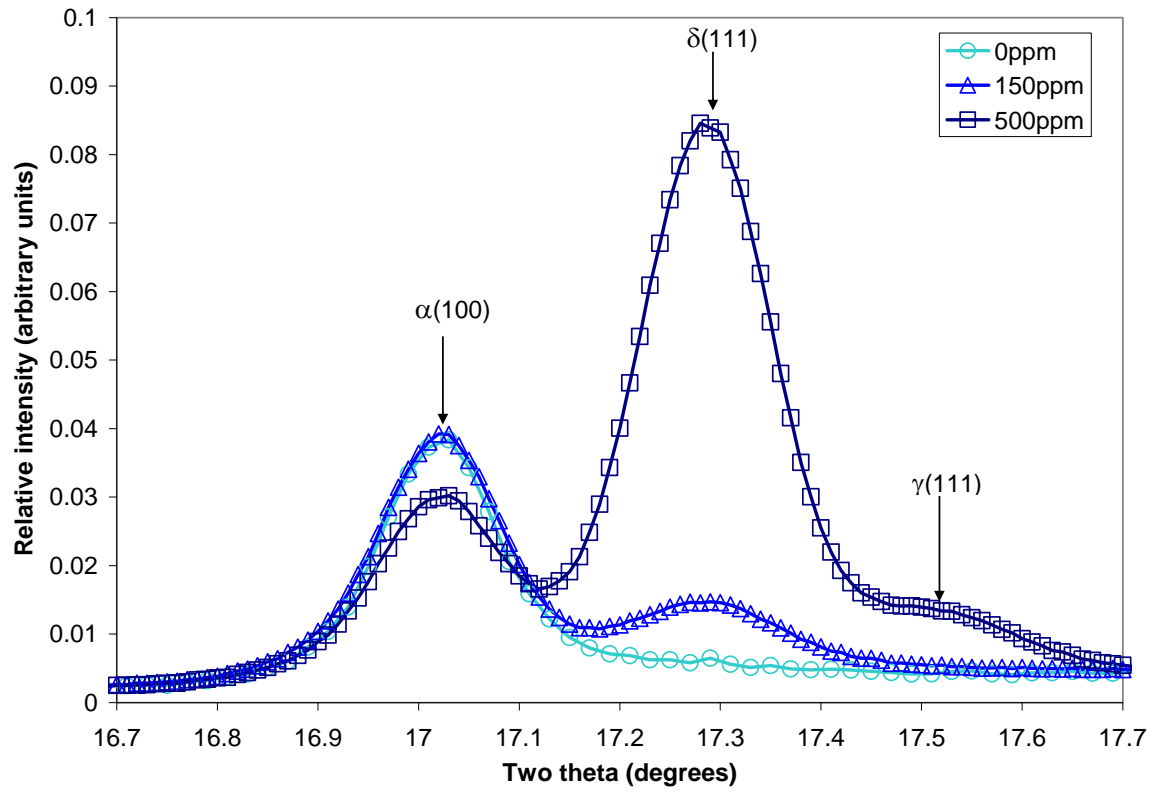


Figure 7: X-ray diffraction patterns of three Zircaloy-2 samples with hydrogen contents of 0 wt.ppm, 150 wt. ppm and 500 wt. ppm.

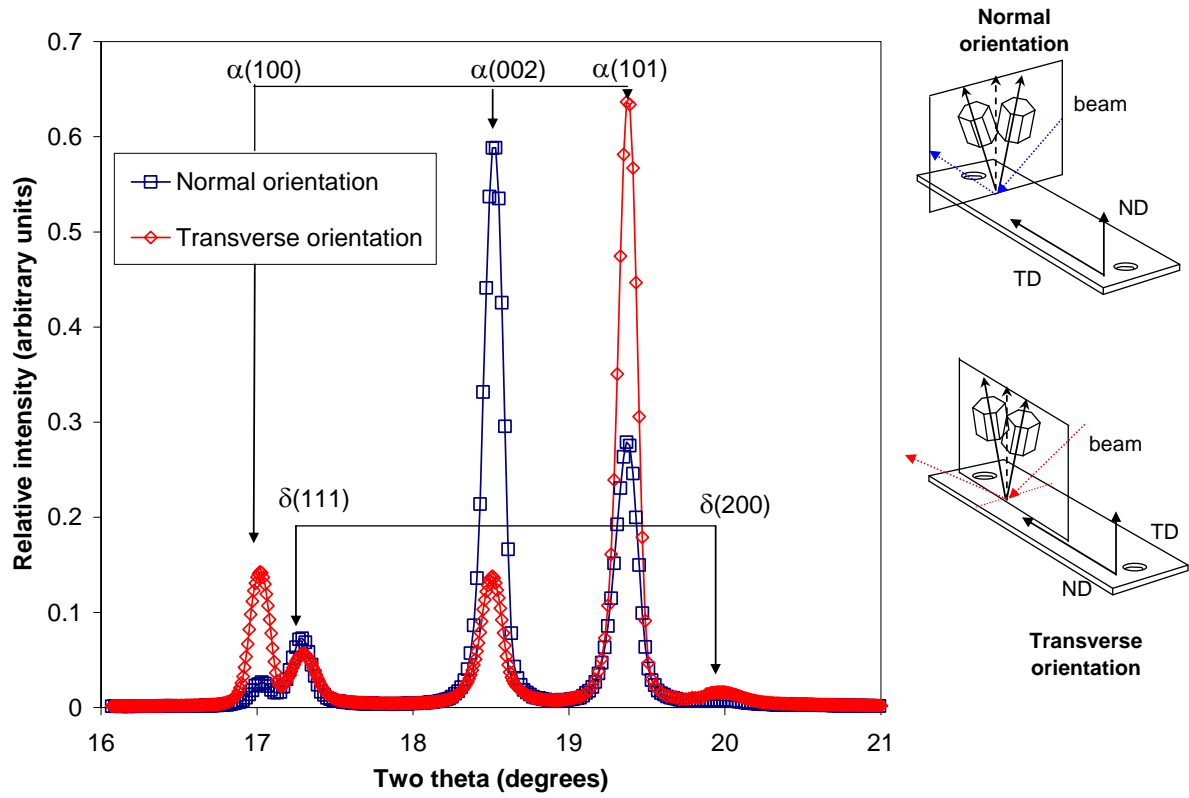


Figure 8: X-ray diffraction patterns of two Zircaloy-2 samples with different microstructural orientation.

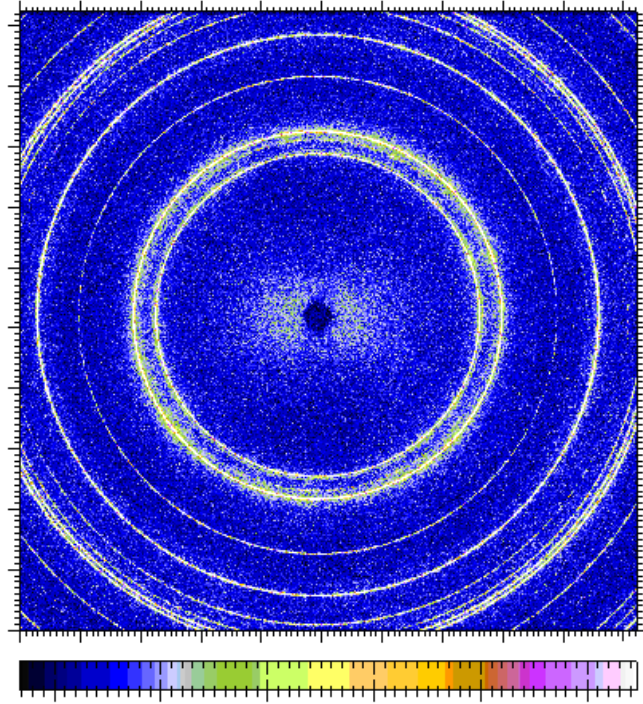


Figure 9: X-ray diffraction data obtained in transmission from a Zircaloy 2 sample with 100 wt. ppm of hydrogen.

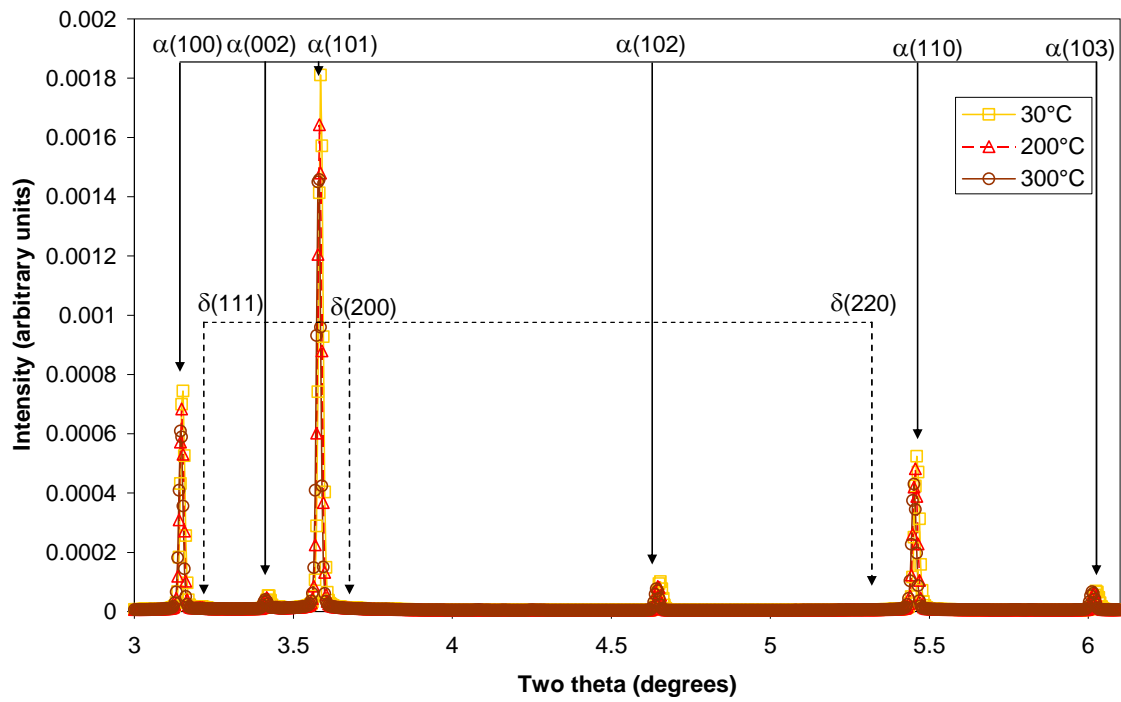


Figure 10: Integrated X-ray diffraction patterns obtained in transmission for a Zircaloy-2 sample with hydrogen content of 100 wt. ppm taken at different temperatures during heating. The indexing for α -zirconium (solid arrows) or δ -hydrides (dashed arrows) peaks is shown.

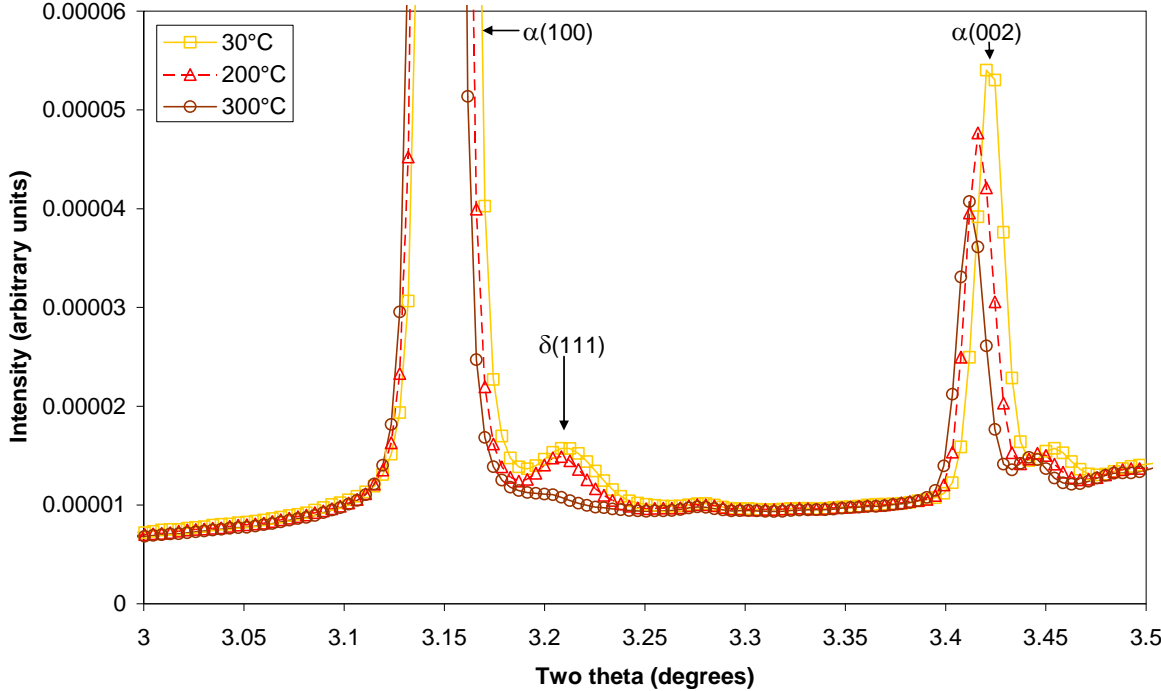


Figure 11: Close-up of Figure 9 integrated diffraction patterns of a Zircaloy-2 sample with hydrogen content of 100 wt.ppm taken at different temperatures during heating.

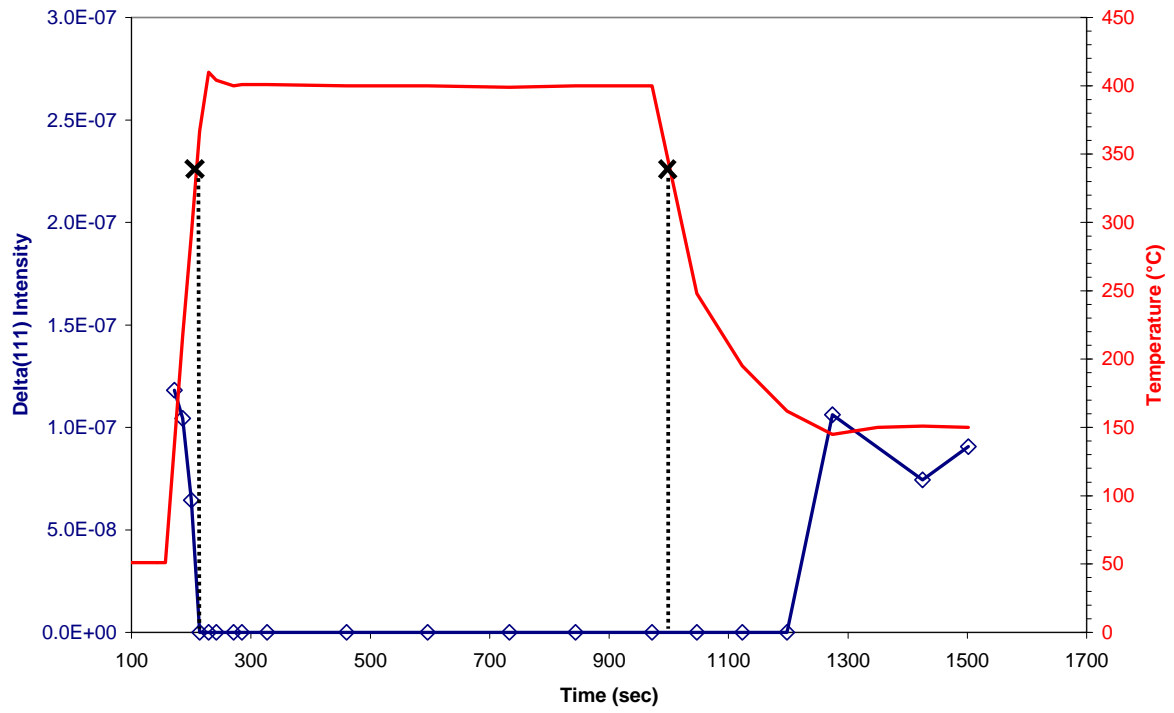


Figure 12: Evolution of delta (111) hydride intensity with time for a Zircaloy-2 sample with 100 ppm in hydrogen content.

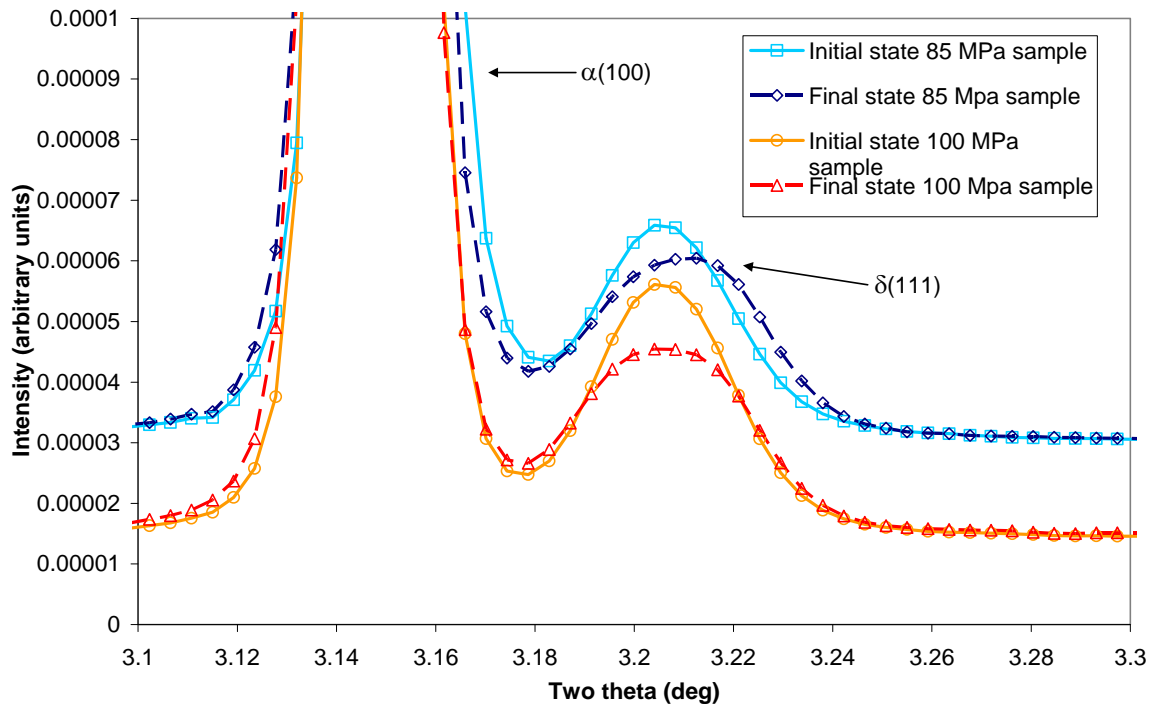


Figure 13: Integrated X-ray diffraction patterns obtained in transmission for two Zircaloy-4 samples before and after heating followed by cooling down under load of 85 MPa and 100 MPa tensile: close-up on $\delta(111)$ peak.

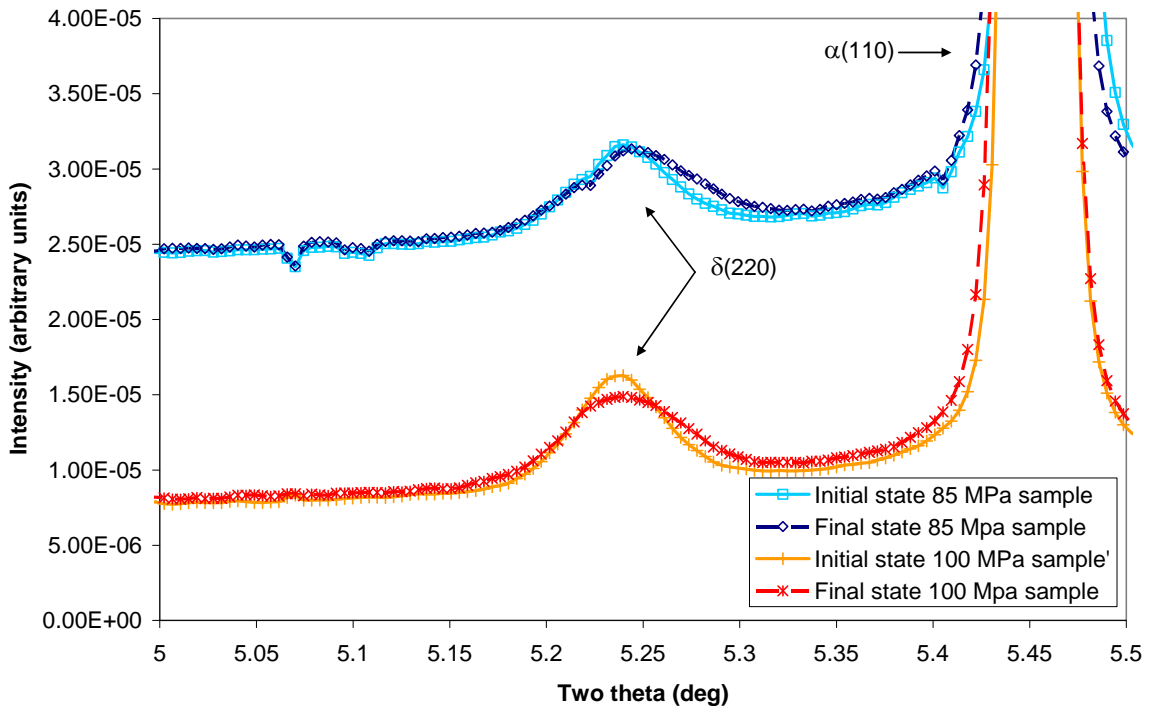


Figure 14: Integrated X-ray diffraction patterns obtained in transmission for two Zircaloy-4 samples before and after heating followed by cooling down under load of 85 MPa and 100 MPa tensile: close-up on $\delta(220)$ peak.